Progress in Solid State Chemistry 76 (2024) 100491

Contents lists available at ScienceDirect

Progress in Solid State Chemistry

journal homepage: www.elsevier.com/locate/pssc

Insights into the structure and polymerization mechanisms of CO molecules under pressure

Xiuyuan Li [a], Zihuan Peng [a], Chongwen Jiang [a], Nan Li [a,*], Jun Zhang [b,**], Changqing Jin [b], Chuan Xiao [a]

[a] State Key Laboratory of Explosion Science and Technology, School of Mechatronical Engineering, Beijing Institute of Technology, Beijing, 100081, PR China
[b] Beijing National Laboratory for Condensed Matter Physics, Institute of Physics, Chinese Academy of Sciences, Beijing, 100190, PR China

A B S T R A C T

High pressure technique can greatly enrich the chemistry research by innovating the traditional research paradigm. Recently, tremendous attentions have been paid to the high-pressure behavior of low-Z molecules, such as CO, CO_2, N_2, O_2 and mixtures. These molecules tend to polymerize into extended solids at the pressure of 1–100 GPa, but the structures and polymerization mechanisms are still poorly understood. Herein, as a research model, high pressure polymerization process of carbon monoxide (CO) is studied in detail both experimentally and theoretically. The in-situ Raman spectra and angle-resolved X-ray diffraction experiments prove the successful synthesis of p-CO and its amorphous structure. The theoretical simulations reveal that two CO molecules dimerize into the ethylenedione (OCCO) diradical with spin-polarized singlet state firstly, then the OCCO diradical induces the subsequent chain elongation, ring closure and chain crosslinking reactions, leading to formation of the amorphous 3D network. The multiple basic units, hybrid coordination of C/O atoms and complex connecting styles in p-CO are revealed. Based on the polymerization mechanisms, the fundamental principles governing the character (amorphous or crystalline) of extended solids under high pressure are elucidated. Due to the small dipole moment and the head-to-tail disorder of CO molecules, it is reasonable to speculate that crystalline p-CO may exist under more rigorous conditions than 110 GPa and 2000 K, at which the isoelectronic nitrogen (N_2) molecules polymerize into a single-bonded cubic form of nitrogen. Our study provides a profound insight into the polymerization mechanism and structures of low-Z CO molecules under compression, contributes to the diversified chemical researches and has a generally scientific implications for the interior dynamics of planets.

1. Introduction

Recently, tremendous attentions have been paid to the high-pressure behavior of low-Z (first- and second-row elements in the periodic table of elements) molecules with unsaturated bonds, such as CO, CO_2, N_2, O_2 and mixtures. By high pressure compressing, these molecules can polymerize into low-Z extended solids, which exhibit unusual properties including superconductivity [1], extreme hardness [2], optically nonlinearity [3] and high energy density [4,5]. Among the low-z molecules, CO is of great importance as an abundant planetary material, which widely distributes in giant planets, interiors of terrestrial planets, interstellar medium, comets and extreme metal-poor galaxies [6,7]. Due to the extreme high-pressure environment there, understanding the behavior of CO molecules under compression is not only a fundamental chemical problem, but also important to explore the initiation stages of planetary formation and the dynamics of planetary interiors. As the polymeric phase of CO under high pressure, the polymeric CO (p-CO) is one of only a few low-Z extended solids that can be recovered to ambient conditions to date [8]. Therefore, CO provides an ideal platform to explore the dynamic process of low-Z molecules under high pressure, including molecular interactions, pressure-induced bonding and growing of clusters.

In 1984, Katz et al. [9] firstly reported the polymerization of CO under compression, then much efforts have been made to reveal the structural information of p-CO. The lactonic rings, bridged O atoms, polycarbonyl chains with conjugated C═C bonds and anhydride groups of p-CO were characterized by comprehensive spectroscopy [10,11]. Also, the p-CO samples synthesized under high pressure (up to 56 GPa) or high temperature (up to 4000 K) were all proved to be amorphous [12–16]. Further experimental exploration and structural characterizations of p-CO is a great challenge due to the metastability and amorphous property as well as the significant noises in spectrograms [8,17]. In that case, theoretical investigations can play an essential role in the deep exploration of p-CO's structures and polymerization mechanisms. So far, several p-CO models with disordered/amorphous property have been simulated through molecular dynamics or geometry optimizations

* Corresponding author.
** Corresponding author.
E-mail addresses: leen04@bit.edu.cn (N. Li), zhang@iphy.ac.cn (J. Zhang).

https://doi.org/10.1016/j.progsolidstchem.2024.100491
Received 27 August 2024; Received in revised form 1 October 2024; Accepted 8 October 2024
Available online 9 October 2024

[18–20], but the polymerization structures and mechanisms of p-CO are still a matter of continuing debate. Therefore, more intensive theoretical researches are of urgent importance.

In this study, the successful synthesis of p-CO and the amorphous structure were proved by the in-situ high pressure spectroscopy experiments, followed by a comprehensive theoretical investigation on the amorphous structures and polymerization mechanisms of p-CO. The 216-atom model of p-CO was constructed by the ab initio molecular dynamics (AIMD) simulations of stepwise compressions on CO liquid, the structural fragments, chemical bonds and hybridization of atoms of p-CO were studied in detail to explore the amorphous property. Density functional theory (DFT) calculations combined with electronic wavefunction analysis were used to reveal the mechanistic and energetic details of the polymerization mechanisms. The detailed polymerization pathway from CO to p-CO (a disordered 3D network) were reasonably proposed. The present work provides deep insights and theoretical clues into the field of high-pressure chemistry and planetary chemistry. Especially, the results will provide valuable reference for the characterizations of amorphous low-Z extended solids and contribute to understand the molecular interactions and pressure-induced bonding.

2. Experimental part

2.1. Sample synthesis and characterizations

The Dimond Anvil Cell (DAC) equipment was employed to prepare the p-CO polymer. And the low temperature encapsulation and high pressure polymerization processes were included. The first essential step is the preparation job about DAC before loading gaseous CO. The culet diameter of diamond anvils is 300 μm. The gasket of T301 stainless was prepressed to the thickness in 40 μm and drilled at the center with a hole of 180 μm in diameter as the high pressure sample chamber. The DAC was clamped with a distance of 5 mm from top to bottom anvil for CO encapsulation. After that, the DAC was sealed in the cryostat and cooled down to 77 K in the liquid nitrogen bath, which connects to the cylinder filled with CO gas. The sample chamber could be filled by liquid CO and then sealed by tightening the DAC. The pressure was applied and determined by measuring the fluorescence peaks of ruby. The p-CO was obtained after compression process.

The Raman spectrum was recorded using an integrated laser Raman system (Renishaw) with a confocal microscope and multichannel air-cooled CCD detector. The excitation source was an Ar ion laser (λ_0 = 532 nm). The high pressure was generated by using a symmetric type diamond-anvil cell (DAC) with 300 μm culets. Angle-resolved high pressure X-ray diffraction experiments were conducted at the Beijing Synchrotron Radiation Facility at room temperature with $\lambda = 0.6199$ Å.

2.2. Computational details

AIMD simulations were performed by CP2K 8.2 package [21] using Gaussian and plane-waves (GPW) approach [22] at the GTH-PBE/DZVP-MOLOPT-SR-GTH [23] level of theory with a cutoff of 1200 Ry. The periodic cells contain 108 CO molecules. The simulations were performed in the NPT ensemble using the Nosé-Hoove thermostat and the DFT-D3 method [24] with the time step of 1 fs. To simulate the stepwise compression of CO, the system of α-CO was initially equilibrated at 1 GPa/300 K for 10 ps, then incrementally compressed to 10 GPa in steps of 1 GPa at 300 K and was equilibrated for 10 ps at each pressure. To ensure the statistical significance of the results, three parallel simulations were performed for each pressure.

Constrained AIMD simulations were performed by the vienna ab initio simulation package (VASP) 5.4 [25–27] using the slow growth approach [28]. Generalized gradient approximation (GGA) with the Perdew-Burke-Ernzerh of (PBE) functional [29] were adopted with a cutoff of 700 eV. The projector augmented planewave method (PAW) is used with hard pseudo-potentials constructed by Blöchl and Kresse [30]. The periodic cells contain 36 CO molecules. The simulations were performed in the NVT ensemble using the Nosé-Hoove thermostat and the DFT-D3 method. Fixed cells with the density of 1.70 g/cm^3 were used to imitate the system at 5 GPa. The temperature was kept at 300 K. An increment of 0.00015 Å/step to collective variables (selected intermolecular C–C, C–O and O–O distance) was applied to drive the reaction. Each simulation was carried out for 10 ps with the time step of 1 fs. The free energy was calculated through integrating the gradients of potential energy.

The single point and frequency calculations of *trans*-bending OCCO was performed with the Gaussian 16 package [31] and the complete active space self-consistent field (CASSCF) method [32,33] at the CASSCF(12,10)/def2-TZVP level of theory [34] to capture its diradical nature. The odd electron density [35,36] was calculated based on the natural orbitals at the CASSCF(2,2)/def2-TZVP level of theory by Multiwfn 3.8 [37], which was also applied to calculate and visualize the inner cavity, molecular electrostatic potential [38] and molecular orbitals. Moreover, the VESTA 3.5.7 [39] and VMD 1.9.3 [40] programs were used to visualize the structure data and trajectories. The R.I.N.G.S. 1.3 code [41] was used to analyze the structures of p-CO.

3. Results and discussion

In this present work, the p-CO sample was successfully synthesized by a high pressure route and proved by the in-situ high pressure Raman and X-ray diffraction experiments. The Raman spectra of CO molecules under pressure were shown in Fig. 1, in which the characteristic peak of CO molecule located at 2138 cm^{-1} appear at the pressure of 1.4 GPa [13], indicating the success of CO encapsulation. As the pressure increases to 6.5 GPa, the characteristic Raman peaks of p-CO centered around 1600 cm^{-1} and 1800 cm^{-1} emerge, which are identified as the C═C and C═O vibrational mode [10,13]. The disappearance of CO molecules and the occurrence of C═C signals in the Raman spectra together indicate the complete transformation of molecular CO to polymerized state. In addition, the angle-resolved high pressure X-ray diffraction experiments were carried out to check the possible structure of the p-CO polymer. Nevertheless, both the X-ray diffraction patterns at 1.7 GPa and 7.4 GPa do not show any diffraction rings or spots, demonstrating the amorphous form of p-CO, which are well consistent with the reported work [15,16]. Thus, it is still a challenge to clarify the complex amorphous structures and polymerization mechanisms of p-CO by experiments. To this end, a comprehensive theoretical investigation on p-CO was carried out in this study.

Based on the AIMD simulations of stepwise compression, it was found that most CO molecules (more than 85 %) gradually polymerized into p-CO at 5 GPa and 300 K. The polymerization condition agrees well with the experimental results [10,12–14]. Considering the similar results of the parallel simulations, one random example at 5 GPa was chosen for the following discussion. Fig. 2 shows the structural evolution as the polymerization reaction proceeding at 5 GPa, which can be divided into three main stages. In stage 1, CO molecules bond with each other through C–C bonds to form chain-like oligomers, which are mainly composed of three-coordinated C and single-coordinated O. In stage 2, partial chain-like oligomers form C_4–O rings and connect with each other through double-coordinated O. In stage 3, all the oligomers merge into a covalent network, and the system transfers to a three-dimensional (3D) network with CO clusters inside. Finally, p-CO shows a disordered 3D network structure with widely distributed inner cavities. The network takes up 85.84 % of the volume of p-CO, while the inner cavities take up 14.16 %. The network structure could be regarded as the combination of chain-like structures and cross-links, while the inner cavities are typically surrounded by single-coordinated O atoms (Fig. 2b). Further structural insight reveals that the p-CO network consists of various basic units, including carbonyl units (c1), tetrahedra units (c2 and c3), ether units (c4), as well as four-membered (r1−r2), five-membered (r3−r9), six-membered (r10−r11) and seven-membered

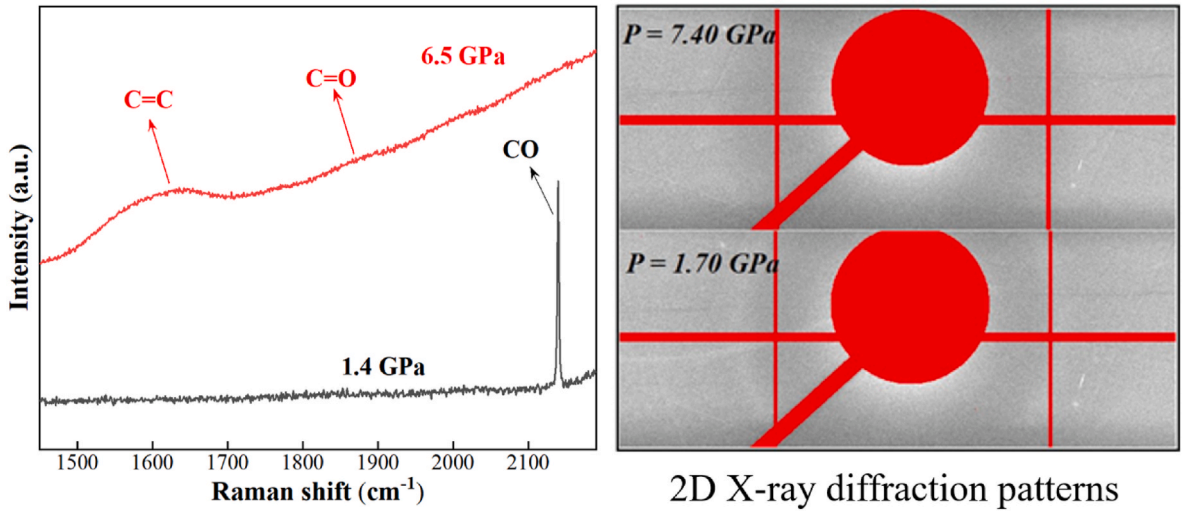

Fig. 1. The Raman spectra of CO samples under pressure and the two-dimensional (2D) X-ray diffraction patterns.

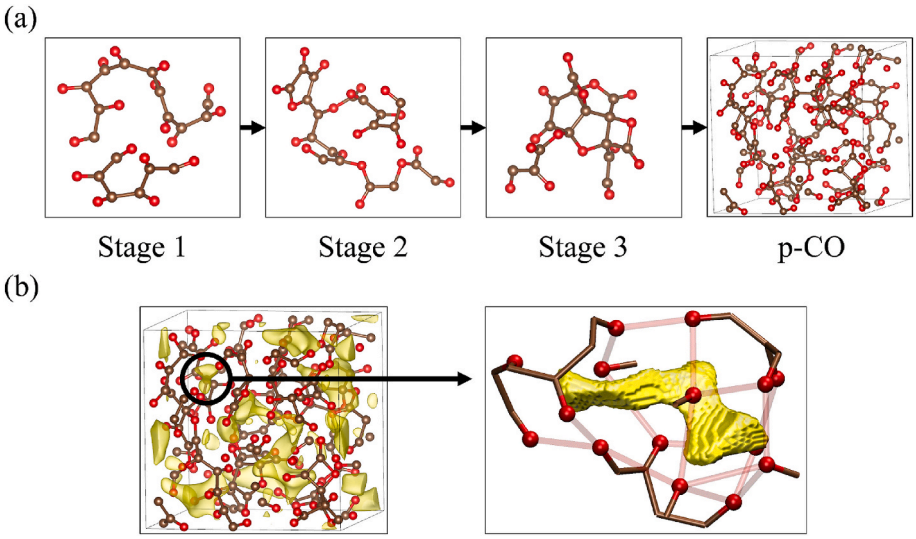

Fig. 2. (a) The typical structures characterizing the distinct stages of polymerization and the snapshot of the amorphous p-CO from the AIMD simulations at 5 GPa and 300 K. The brown and red balls denote C and O atoms, respectively. (b) The left panel shows all the inner cavities (yellow isosurface) in p-CO. The isosurface was calculated by promolecular density (isovalue = 0.0017). The detailed structure of one of the cavities is shown in the right panel. The C atoms are omitted for clarity, and single coordinated O atoms are connected by transparent red sticks to emphasize this cavity.

ring units (r12), as shown in Fig. 3a. The chain-like structures are composed of the units c1, c4, r1 and r8, and the cross-links include the rest units, as shown in Fig. 3b. Most of these units are multiple lactonic rings, some of which have been characterized in experiment [13].

The chemical bonds of p-CO are characterized by the radial distribution function (RDF) and coordinate number (CN). As shown in Fig. 4, RDF and CN were calculated for atom pairs C–O (Fig. 4a), C–C (Fig. 4b) and O–O (Fig. 4c) in both the molecular phase and the polymeric phase at 5 GPa. Comparing to the RDF of molecular phase, there are some new peaks emerging in that of polymeric phase, implying the formation of new bonds. For C–O pair, besides C≡O bond, the C═O and C–O bonds with the new peaks located at 1.21 Å and 1.38 Å are also proved and the ratio of C≡ O, C═O and C–O bonds is 6.45: 54.84: 38.71 supported by the CN of 0.08, 0.68 and 0.48. For C–C pair, two new RDF peaks of 1.35 Å and 1.52 Å emerge, which indicates the formation of C═C and C–C bonds. Their CNs of 0.10 and 1.74 respectively implies C═C amounts to 5.75 % and C–C bonds 94.25 %. No C ≡C bond exists in the polymeric phase. For O–O pair, no peak of RDF located within 2.00 Å for polymeric phase, indicating the absence of O–O bonds in p-CO. Also, to date all the experimental characterizations of p-CO have not found the existence of O–O bonds [10–16]. Here, C and O atoms both present two types of coordination, in which the C atoms are three- and four-coordinated, and the O atoms are single- and double-coordinated, respectively. According to the CN results for C–O and C–C atom pairs, the 3D network of p-CO is composed of C–C (56.55 %), C═O (23.45 %), C–O (16.55 %) and a few C═C (3.45 %) bonds. Interestingly, all the few C═C bonds only exist in the five-membered rings (r7 and r8 in Fig. 3). Therefore, it is speculated that the ring tension force of four-membered rings or the non-planar configuration of six- and seven-membered rings is neither favorable for C═C bonds. Above results well agree with the experimental conclusions that three-coordinated C and single-coordinated O are the major components of p-CO [15]. In conclusion, multiple basic units, hybrid coordination of C/O atoms, and complicated connecting styles result in the disordered 3D network structure of p-CO.

High pressure can lead to the decrease of intermolecular distance and increase of intermolecular interaction. According to the present simulations, high pressure of 5 GPa and thermal fluctuations at 300 K [42,43] can induce the strong interaction between adjacent CO molecules,

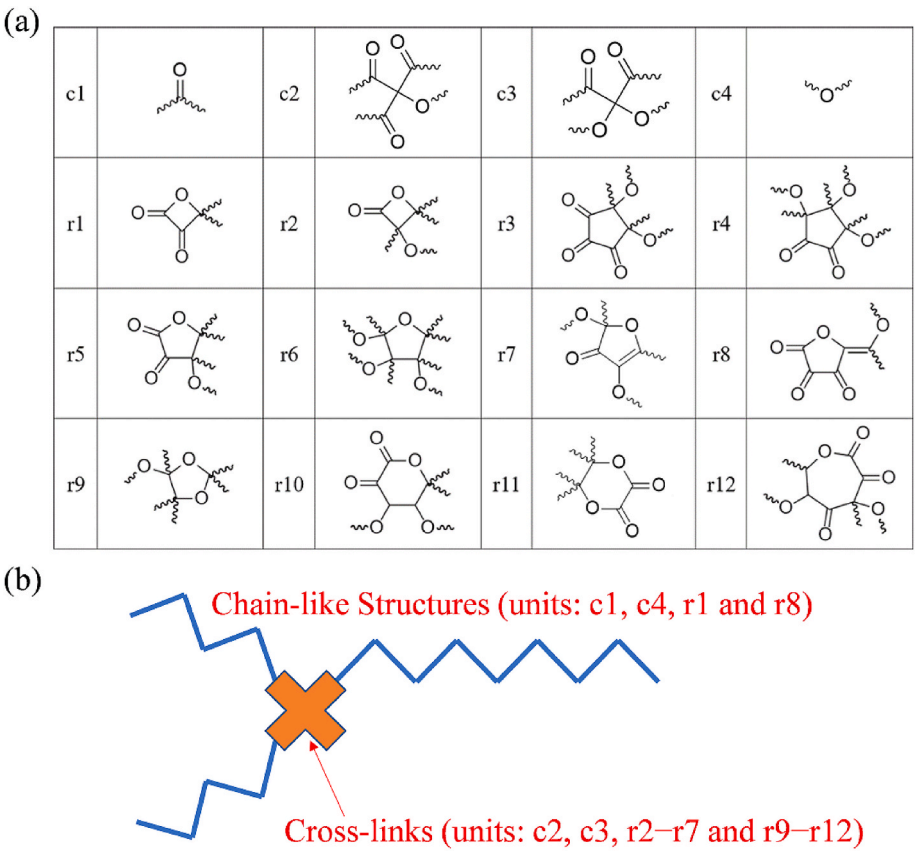

Fig. 3. The basic units and their organization in p-CO. (a) The basic units of the 3D network structure (c1−c4 and r1−r12), which are connected to the p-CO backbone at the wavy bond. (b) Diagram of the 3D network structure of p-CO.

resulting in the dimerization of CO. In this process, it was observed for the first time that CO can directly dimerize into ethylenedione (OCCO) through C–C bonds, which was further defined by comparing the free energy barriers of three possible bonding schemes of CO dimerization (Fig. S1 of the supplementary material). The concrete dimerization mechanism of OCCO at 5 GPa is illustrated in Fig. 5. At the beginning, two CO molecules (respectively named as C1O1 and C2O2) tend to approach each other in a complementary manner of molecular electrostatic potential (MEP) [44], where the positive part of one CO significantly overlaps with the negative part of another CO (Fig. 5a). Thus, C1O1 and C2O2 are restricted to a *trans*-bending configuration with the O1–C1–C2 and O2–C2–C1 angles of 125° and the O1–C1–C2–O2 dihedral angle of 0°. Once formed, this *trans*-bending configuration remains throughout the whole dimerization process (Fig. 5b and Fig. S2 of the supplementary material). It is well known that C and O of CO molecule both have two *sp* and two *p* orbitals, where the weakest bond is the dative π bond composed of the full *p* orbital of O atom and empty *p* orbital of C atom. In the further approaching, the strong interaction of C1O1 and C2O2 leads to the cleavage of the dative bond. Meanwhile, the *sp*-to-sp^2 hybridization transformation and electron rearrangement for both C1/C2 and O1/O2 atoms happen. As shown in Fig. 5b, besides the orbitals forming the C1═O1 and C2═O2 bonds, there are still two half-full sp^2 orbitals for each C atom. One of the sp^2 orbitals of C1/C2 atom is used to form the C1–C2 σ bond and produces the O1C1C2O2 molecule, and the left orbitals endow the OCCO one unpaired electron on each C atom, which can be proved and visualized clearly by the odd electron density (OED) analysis. Interestingly, according to the single-point calculations, the energy of diradical OCCO in singlet state is about 180 kJ/mol lower than that in triplet state. Therefore, it can be reasonably inferred that the OCCO in our simulation should be the spin-polarized singlet state, whose two unpaired electrons have opposite spin directions. Our simulation reveals that at 5 GPa and 300 K two CO molecules can directly dimerize into the *trans*-bending OCCO in spin-polarized singlet state (Fig. 5c). In fact, OCCO is also the possible intermediate of ambient pressure reactions, such as the dehydrogenation of glyoxal [45], the reaction between oxalyl bromide and mercury [46] or between carbon and carbon dioxide [47]. It has been theoretically studied [45–51] for decades at ambient pressure condition. Nevertheless, in these reports, the global minimum of OCCO has the linear configuration with triplet state (Fig. 5d), which is different from the OCCO observed in our simulation. Therefore, the high pressure acting as the strong intermolecular interaction plays a critical role to produce and stabilize this OCCO with special geometric and electronic structure. Our results demonstrate the great potential of utilizing high-pressure to explore new states of matter.

The further polymerization reaction occurs between OCCO and CO to form C_3O_3. As presented in Fig. 6a, the OCCO ($OC^{\bullet}C^{\bullet}O$) attack the adjacent CO, leading to the cleavage of CO's dative bond and the corresponding *sp*-to-sp^2 hybridization transformation. Similarly, for the C atom of this CO, besides the orbitals forming the C═O bonds, there are still two half-full sp^2 orbitals. One overlaps with one half-full sp^2 orbital of OCCO to form the new C–C bond, producing the C_3O_3 ($OC^{\bullet}(C=O)C^{\bullet}O$) molecule, while the other remains unpaired. Therefore, the C_3O_3 still have one unpaired electron on each end C atom. This process is concluded as $OC^{\bullet}C^{\bullet}O + CO \rightarrow OC^{\bullet} - (C=O) - C^{\bullet}O$. Based on the analogous mechanisms, the growth of chain-like oligomers proceeds through the successive formation of C–C bonds with adjacent CO (Fig. 6b), and these oligomers all have one unpaired electron on each end C atom. These chain elongation reactions can be concluded as $OC^{\bullet}-(C=O)_{n-1} - C^{\bullet}O + CO \rightarrow OC^{\bullet} - (C=O)_n - C^{\bullet}O$. Among these oligomers, only C_2O_2 and C_3O_3 are nearly planar, while others are non-planar due to the repulsion of O atoms and multiple rotatable C–C bonds.

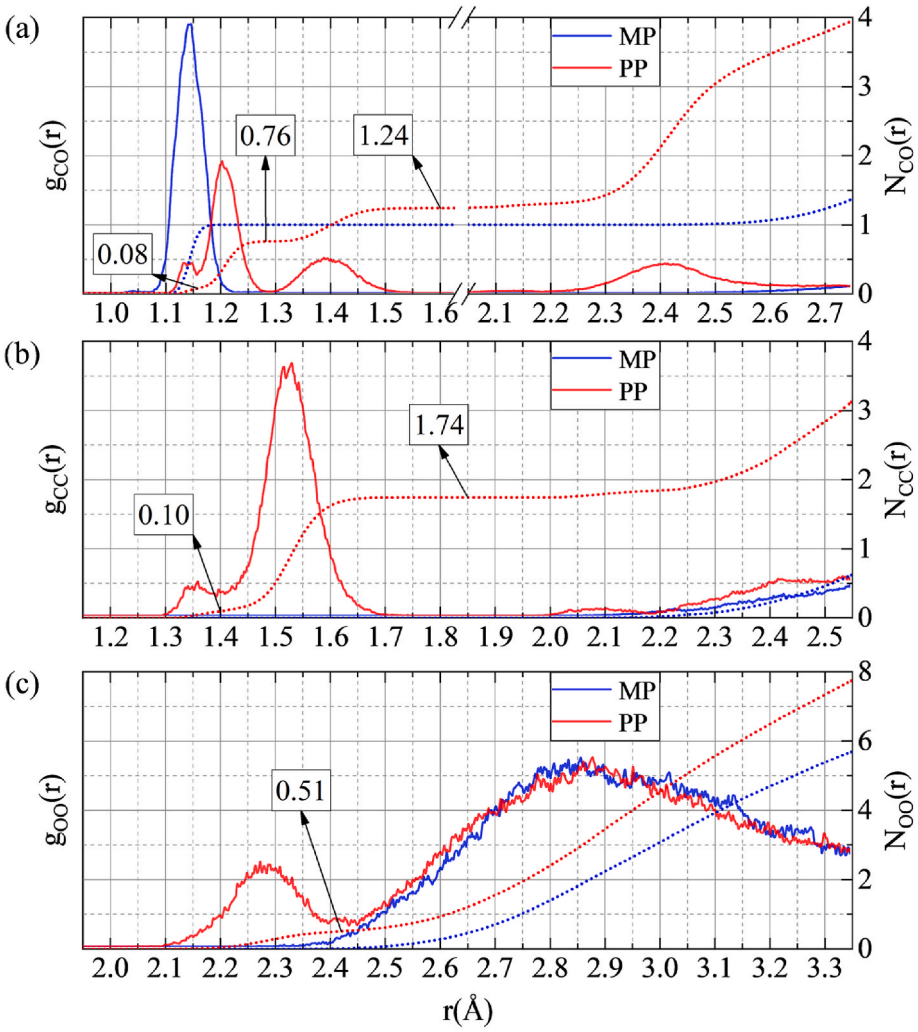

Fig. 4. The radial distribution function (solid lines) and coordination number (dot lines) curves of C–O (a), C–C (b) and O–O (c) pairs in the CO molecular phase (MP) and the p-CO polymeric phase (PP) under 5 GPa.

The C═O stretching mode centered around 1800 cm^{-1} in the Raman spectroscopy was observed in synthesized p-CO, which backed up the structure predicted by theoretical simulations.

Besides chain-like oligomers, multiple four-, five-, six-, and seven-membered rings were also observed during the polymerization, and the related processes are denoted as ring closure reactions. Here we take the formation of five-membered rings as an example to explain the corresponding mechanisms (Fig. 7). The unpaired electron of the C atom at the chain end attacks the carbonyl O atom from the same chain, forming the C–O bond and the five-membered lactonic ring. During this process in Fig. 7a, it is clear that the unpaired electron transfers through a series of bonding reaction, successively the oxygen bridge, C═C bond and C–O bond, finally to another carbonyl O atom of this chain. Similarly, as shown in Fig. 7b, the unpaired electron attacks the carbonyl C atom from the same chain, forming the five-membered ring and radical O. For comparing to the C atoms, the O atoms are always lie on the outer sides of backbone of oligomers and easier to be attacked by the radicals. Overall, in our simulation, the ring closure reactions can take place for all the chain-like oligomers with different chain lengths (from C_4O_4 to $C_{17}O_{17}$) and produce diverse rings.

At last, the 3D covalent network of p-CO was constructed via two kinds of chain crosslinking reactions (Fig. 7c and d) and subsequent radical elimination. The mechanisms of chain crosslinking reactions are similar with those of ring closure reactions. In Fig. 7c, the unpaired electron of the C atom at the chain end attacks the carbonyl O atom of another chain, forming a C–O bond and a radical C atom. In Fig. 7d, the unpaired electron attacks the carbonyl C atom of another chain, forming a C–C bond and a radical O atom. These chain crosslinking reactions connect all the oligomers to produce a loose network of p-CO, and further reactions between the radicals form more C–C and C–O bonds, resulting in a bigger interconnected network structure. In addition, it is believed the complicated network plays a key role in the recoverability of p-CO.

Some efforts have been made to search for the p-CO crystalline phases both theoretically [52–56] and experimentally [12,15,16]. However, almost all the p-CO samples characterized experimentally are amorphous. A recent study attempted to synthesize crystalline p-CO through high temperature annealing of amorphous p-CO but failed [16]. Based on the abovementioned polymerization mechanisms, we could predict roughly the possibility of obtaining crystalline p-CO. The phase diagram of CO in Fig. 8 shows that most CO molecular phases adjacent to p-CO phase are disordered (fluid, β-CO or δ-CO), which cannot facilitate the formation of crystalline p-CO. Although the ε-CO phase is ordered, it still transforms into p-CO amorphous phase under compression [11]. This could be ascribed to small dipole moment (0.122 D) of CO molecules [57], which also results in the weak intermolecular interaction among CO molecules. During the compression process, the CO molecules with weak intermolecular interaction are difficultly aligned or orientated in ordered configurations. Thereby, p-CO in amorphous phase is favorable in energy than crystalline p-CO. Furthermore, the head-to-tail

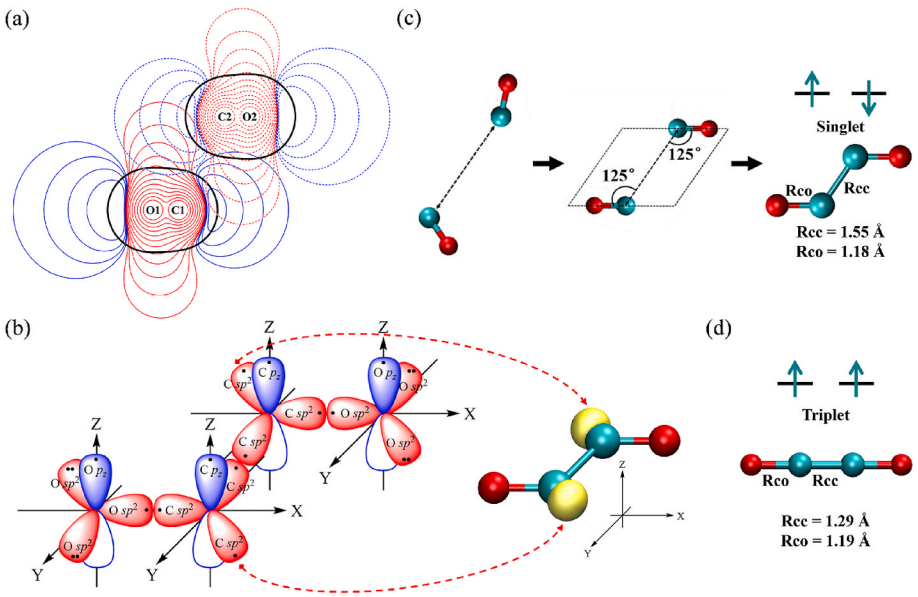

Fig. 5. The mechanisms of CO dimerization. (a) Overlapping map of CO's MEP. Positive and negative parts of C1O1/C2O2 are represented as red and blue solid/dash lines, respectively. The black lines correspond to Bader's vdW surface, namely the isosurface of 0.001 a.u. electron density. (b) Hybrid orbitals (on the left) of *trans*-bending OCCO. The red and blue lobes denote sp^2 and *p* orbitals, respectively. Each black points in the lobes denotes one electron. OED distributions (yellow isosurface on the right) of singlet *trans*-bending OCCO calculated by the CASSCF method (isovalue = 0.01 arb. units). The cyan and red balls denote C and O atoms, respectively. (c) The formation of *trans*-bending configuration during the dimerization process. The R_{CC} and R_{CO} are obtained from the AIMD average structure of OCCO. The cyan and red balls denote C and O atoms, respectively. (d) The linear configuration of OCCO with triplet state predicted in Ref. [51].

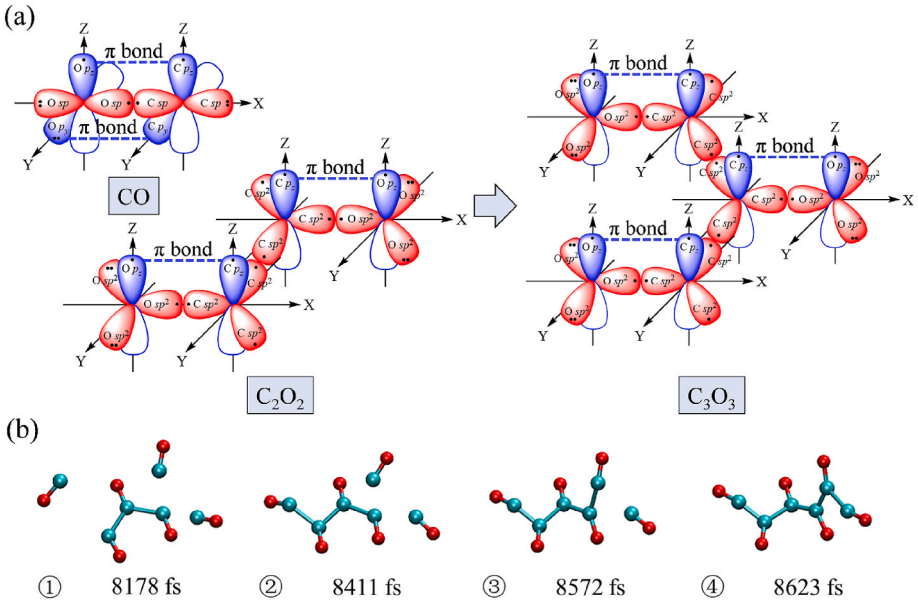

Fig. 6. The mechanisms of chain elongation reactions. (a) Hybrid orbitals of CO, C_2O_2 and C_3O_3 during the formation of C_3O_3. The red and blue lobes denote sp^2 and *p* orbitals, respectively. The black points in each lobe denote unpaired electrons. (b) Snapshots of the chain elongation reactions from C_3O_3 to C_6O_6 in the AIMD simulation at 5 GPa and 300 K. The cyan and red balls denote C and O atoms, respectively.

disorder of CO impose significant hurdle for the polymerization or transformation into crystalline p-CO. Considering that N_2 molecules, which have high molecular symmetry and zero dipole moment, can polymerize into a crystalline cubic gauche nitrogen or (cg-N) at 110 GPa and 2000 K [4]. It is speculated that the crystalline p-CO may exist under more extreme conditions, like the interior of giant planets.

4. Conclusion

In this study, the pressure-induced polymerization process of CO molecules was elucidated by the combined experimental and theoretical approaches. The dimerization of CO molecules initializes the polymeric reaction and product OCCO with unusual geometry and electronic structure. The diradical-induced chain elongation, ring closure and chain crosslinking reactions lead to the structure growth into the amorphous 3D network. The present results reveal the multiple basic units, hybrid coordination of C/O atoms and complicated connecting styles of amorphous p-CO, in which three-coordinated C and single-coordinated O are the major components of p-CO. Furthermore, the characters of CO's molecular phases, the small dipole moment and the

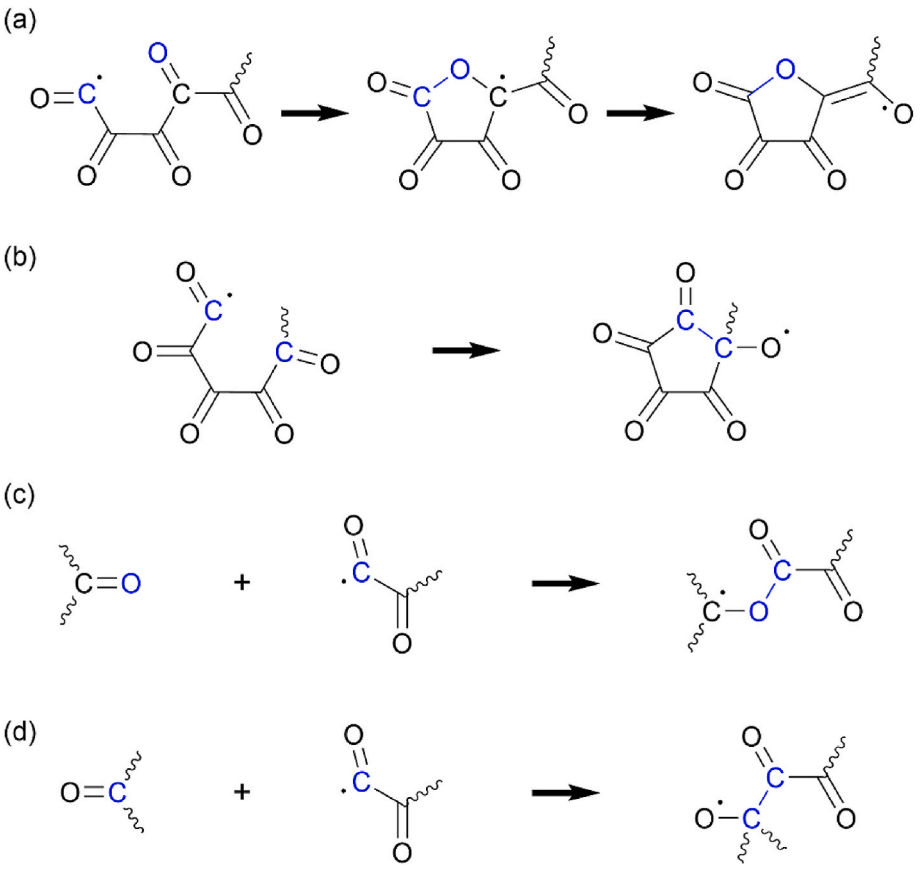

Fig. 7. The reaction mechanisms of ring closure reactions (a and b) and chain crosslinking reactions (c and d). All the fragments are connected to the oligomers at the wavy bond.

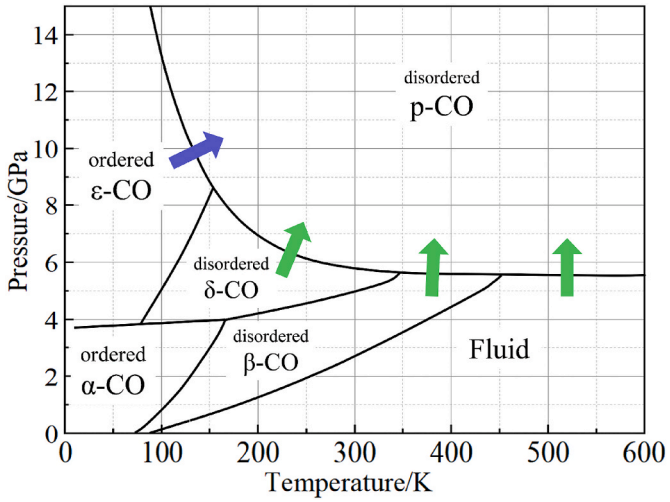

Fig. 8. Phase diagram of CO constructed by the data in Ref. [11]. The four arrows indicate possible phase transitions from CO into p-CO.

head-to-tail disorder of CO molecule make the formation of crystalline p-CO so challenging, which may exist under conditions more extreme than those required to synthesize cg-N (110 GPa/2000 K). Our results give some important inspiration for high-pressure chemistry and planetary chemistry. Meanwhile, understanding the pressure-induced polymerization of p-CO offers new insights into the development of ambient stabilization of low-Z extended solids and illuminates their potential applications.

CRediT authorship contribution statement

Xiuyuan Li: Writing – original draft, Investigation, Formal analysis, Data curation, Conceptualization. **Zihuan Peng:** Investigation, Data curation. **Chongwen Jiang:** Investigation, Formal analysis, Data curation. **Nan Li:** Writing – review & editing, Writing – original draft, Supervision, Formal analysis, Data curation, Conceptualization. **Jun Zhang:** Writing – review & editing, Supervision, Conceptualization. **Changqing Jin:** Writing – review & editing, Supervision, Conceptualization. **Chuan Xiao:** Supervision, Conceptualization.

Data availability statement

The data that support the findings of this study are available within this article and its supplementary material.

Declaration of competing interest

The authors declare that they have no known competing financial interests or personal relationships that could have appeared to influence the work reported in this paper.

Acknowledgements

The authors acknowledge the financial support by the Basic Research Strengthening Program of China under Grant 2023-JCJQ-JJ-0248. This work used computational resources by the National Supercomputing Center in Shenzhen.

Appendix A. Supplementary data

Supplementary data to this article can be found online at https://doi.org/10.1016/j.progsolidstchem.2024.100491.

References

[1] Eremets MI, Struzhkin VV, Mao H-k, Hemley RJ. Exploring superconductivity in low-Z materials at megabar pressures. Physica B 2003;329:1312–6.
[2] Yamanaka S, Kini NS, Kubo A, Jida S, Kuramoto H. Topochemical 3D polymerization of C60 under high pressure at elevated temperatures. J Am Chem Soc 2008;130:4303–9.
[3] Iota V, Yoo C, Cynn H. Quartzlike carbon dioxide: an optically nonlinear extended solid at high pressures and temperatures. Science 1999;283:1510–3.
[4] Eremets MI, Gavriliuk AG, Trojan IA, Dzivenko DA, Boehler R. Single-bonded cubic form of nitrogen. Nat Mater 2004;3:558–63.
[5] Mao H-K, Ji C, Li B, Liu G, Gregoryanz E. Extreme energetic materials at ultrahigh pressures. Engineering 2020;6:976–80.
[6] Shi Y, Wang J, Zhang Z-Y, Gao Y, Hao C-N, Xia X-Y, Gu Q. Carbon monoxide in an extremely metal-poor galaxy. Nat Commun 2016;7:13789.
[7] Leonhardi TC, Militzer B. Ab initio simulations of liquid carbon monoxide at high pressure. High Energy Density Phys 2017;22:41–5.
[8] Yoo C-S. Chemistry under extreme conditions: pressure evolution of chemical bonding and structure in dense solids. Matter Radiat. Extrem. 2020;5:018202.
[9] Mills R, Schiferl D, Katz A, Olinger B. New phases and chemical reactions in solid CO under pressure. J Phys Colloq 1984;45. C8-187-C188-190.
[10] Lipp MJ, Evans WJ, Baer BJ, Yoo C-S. High-energy-density extended CO solid. Nat Mater 2005;4:211–5.
[11] Ceppatelli M, Serdyukov A, Bini R, Jodl HJ. Pressure induced reactivity of solid CO by FTIR studies. J Phys Chem B 2009;113:6652–60.
[12] Ryu Y-J, Kim M, Lim J, Dias R, Klug D, Yoo C-S. Dense carbon monoxide to 160 GPa: stepwise polymerization to two-dimensional layered solid. J Phys Chem C 2016;120:27548–54.
[13] Evans W, Lipp M, Yoo C-S, Cynn H, Herberg J, Maxwell R, Nicol M. Pressure-induced polymerization of carbon monoxide: disproportionation and synthesis of an energetic lactonic polymer. Chem Mater 2006;18:2520–31.
[14] Dang NC, Ciezak-Jenkins JA. Kinetic effects on the morphology and stability of the pressure-induced extended-solid of carbon monoxide. J Chem Phys 2018;148:144702.
[15] Santoro M, Bini R, Ceppatelli M, Garbarino G, Gorelli FA, Hanfland M, Scelta D. High pressure structural changes in amorphous polymeric carbon monoxide by combined infrared spectroscopy and X-ray diffraction. J Phys Chem C 2022;126:11840–5.
[16] Scelta D, Ceppatelli M, Bini R, Pakhomova A, Garbarino G, Mezouar M, Santoro M. High temperature decomposition of polymeric carbon monoxide at pressures up to 120 GPa. J Chem Phys 2023;159.
[17] Shieh SR, Jarrige I, Wu M, Hiraoka N, Tse JS, Mi Z, Kaci L, Jiang J-Z, Cai YQ. Electronic structure of carbon dioxide under pressure and insights into the molecular-to-nonmolecular transition. Proc. Natl. Acad. Sci. 2013;110:18402–6.
[18] Bernard S, Chiarotti GL, Scandolo S, Tosatti E. Decomposition and polymerization of solid carbon monoxide under pressure. Phys Rev Lett 1998;81:2092.
[19] Rademacher N, Bayarjargal L, Morgenroth W, Winkler B, Ciezak-Jenkins J, Batyrev IG, Milman V. The local atomic structures of liquid CO at 3.6 GPa and polymerized CO at 0 to 30 GPa from high-pressure pair distribution function analysis. Chem.–Eur. J. 2014;20:11531–9.
[20] Bonev S, Lipp M, Crowhurst J, McCarrick J. Energetics of polymeric carbon monoxide. J Chem Phys 2021;155:054501.
[21] VandeVondele J, Krack M, Mohamed F, Parrinello M, Chassaing T, Hutter J. Quickstep: fast and accurate density functional calculations using a mixed Gaussian and plane waves approach. Comput Phys Commun 2005;167:103–28.
[22] Lippert BG, Parrinello JH. MICHELE, A hybrid Gaussian and plane wave density functional scheme. Mol Phys 1997;92:477–88.
[23] VandeVondele J, Hutter J. Gaussian basis sets for accurate calculations on molecular systems in gas and condensed phases. J Chem Phys 2007;127:114105.
[24] Grimme S, Antony J, Ehrlich S, Krieg H. A consistent and accurate ab initio parametrization of density functional dispersion correction (DFT-D) for the 94 elements H-Pu. J Chem Phys 2010;132:154104.
[25] Kresse G, Hafner J. Ab initio molecular dynamics for liquid metals. Phys Rev B 1993;47:558.
[26] Kresse G, Furthmüller J. Efficient iterative schemes for ab initio total-energy calculations using a plane-wave basis set. Phys Rev B 1996;54:11169.
[27] Kresse G, Joubert D. From ultrasoft pseudopotentials to the projector augmented-wave method. Phys Rev B 1999;59:1758.
[28] Woo TK, Margl PM, Blöchl PE, Ziegler T. A combined Car− parrinello QM/MM implementation for ab initio molecular dynamics simulations of extended systems: application to transition metal catalysis. J Phys Chem B 1997;101:7877–80.
[29] Perdew JP, Burke K, Ernzerhof M. Generalized gradient approximation made simple. Phys Rev Lett 1996;77:3865.
[30] Blöchl PE. Projector augmented-wave method. Phys Rev B 1994;50:17953.
[31] Frisch MJ, Trucks GW, Schlegel HB, Scuseria GE, Robb MA, Cheeseman JR, Scalmani G, Barone V, Petersson GA, Nakatsuji H, Li X, Caricato M, Marenich AV, Bloino J, Janesko BG, Gomperts R, Mennucci B, Hratchian HP, Ortiz JV, Izmaylov AF, Sonnenberg JL, Williams, Ding F, Lipparini F, Egidi F, Goings J, Peng B, Petrone A, Henderson T, Ranasinghe D, Zakrzewski VG, Gao J, Rega N, Zheng G, Liang W, Hada M, Ehara M, Toyota K, Fukuda R, Hasegawa J, Ishida M, Nakajima T, Honda Y, Kitao O, Nakai H, Vreven T, Throssell K, Montgomery Jr JA, Peralta JE, Ogliaro F, Bearpark MJ, Heyd JJ, Brothers EN, Kudin KN, Staroverov VN, Keith TA, Kobayashi R, Normand J, Raghavachari K, Rendell AP, Burant JC, Iyengar SS, Tomasi J, Cossi M, Millam JM, Klene M, Adamo C, Cammi R, Ochterski JW, Martin RL, Morokuma K, Farkas O, Foresman JB, Fox DJ. Gaussian 16 rev. C.01. Journal 2016.
[32] Knowles P, Sexton G, Handy N. Studies using the CASSCF wavefunction. Chem Phys 1982;72:337–47.
[33] Roos BO, Taylor PR, Sigbahn PE. A complete active space SCF method (CASSCF) using a density matrix formulated super-CI approach. Chem Phys 1980;48:157–73.
[34] Weigend F, Ahlrichs R. Balanced basis sets of split valence, triple zeta valence and quadruple zeta valence quality for H to Rn: design and assessment of accuracy. Phys Chem Chem Phys 2005;7:3297–305.
[35] Takatsuka K, Fueno T, Yamaguchi K. Distribution of odd electrons in ground-state molecules. Theor Chim Acta 1978;48:175–83.
[36] Nakano M, Fukui H, Minami T, Yoneda K, Shigeta Y, Kishi R, Champagne B, Botek E, Kubo T, Ohta K. Hyper) polarizability density analysis for open-shell molecular systems based on natural orbitals and occupation numbers. Theor Chem Acc 2011;130:711–24.
[37] Lu T, Chen F. Multiwfn: a multifunctional wavefunction analyzer. J Comput Chem 2012;33:580–92.
[38] Zhang J, Lu T. Efficient evaluation of electrostatic potential with computerized optimized code. Phys Chem Chem Phys 2021;23:20323–8.
[39] Momma K, Izumi F. VESTA 3 for three-dimensional visualization of crystal, volumetric and morphology data. J Appl Crystallogr 2011;44:1272–6.
[40] Humphrey W, Dalke A, Schulten K. VMD: visual molecular dynamics. J Mol Graph 1996;14:33–8.
[41] Le Roux S, Jund P. Ring statistics analysis of topological networks: new approach and application to amorphous GeS2 and SiO2 systems. Comp. Mater. Sci. 2010;49:70–83.
[42] Mugnai M, Cardini G, Schettino V. High pressure reactivity of propene by first principles molecular dynamics calculations. J Chem Phys 2004;120:5327–33.
[43] Mugnai M, Pagliai M, Cardini G, Schettino V. Mechanism of the ethylene polymerization at very high pressure. J. Chem. Theory Comput. 2008;4:646–51.
[44] Lu T, Chen F. Revealing the nature of intermolecular interaction and configurational preference of the nonpolar molecular dimers (H2) 2,(N2) 2, and (H2)(N2). J Mol Model 2013;19:5387–95.
[45] Dixon AR, Xue T, Sanov A. Spectroscopy of ethylenedione. Angew. Chem.-Int. Edit. 2015;54:8764–7.
[46] Staudinger H, Anthes E, Oxalylchlorid V. Über Oxalylbromid und Versuche zur Darstellung von Di-Kohlenoxyd. Ber Dtsch Chem Ges 1913;46:1426–37.
[47] Krasnokutski SA, Tkachenko O, Jäger C, Henning T. Formation of a long-lived cyclic isomer of ethylenedione. Phys Chem Chem Phys 2019;21:12986–90.
[48] Korkin AA, Balkova A, Bartlett RJ, Boyd RJ, Schleyer PvR. The 28-electron tetraatomic molecules: N4, CN2O, BFN2, C2O2, B2F2, CBFO, C2FN, and BNO2. Challenges for computational and experimental chemistry. J. Phys. Chem. 1996;100:5702–14.
[49] Schröder D, Heinemann C, Schwarz H, Harvey JN, Dua S, Blanksby SJ, Bowie JH. Ethylenedione: an intrinsically short-lived molecule. Chem.–Eur. J. 1998;4:2550–7.
[50] Talbi D, Chandler GS. Extensive ab initio study of the C2O2, C2S2, and C2OS systems: stabilities and Singlet−Triplet energy gaps. J Phys Chem A 2000;104:5872–81.
[51] Mato J, Poole D, Gordon MS. Stability and dissociation of ethylenedione (OCCO). J Phys Chem A 2020;124:8209–22.
[52] Sun J, Klug DD, Pickard CJ, Needs RJ. Controlling the bonding and band gaps of solid carbon monoxide with pressure. Phys Rev Lett 2011;106:145502.
[53] Xia K, Sun J, Pickard CJ, Klug DD, Needs RJ. Ground state structure of high-energy-density polymeric carbon monoxide. Phys Rev B 2017;95:144102.
[54] Sun C, Guo W, Zhu J, Li X, Yao Y. High-energy-density polymeric carbon oxide: layered C x O y solids under pressure. Phys Rev B 2021;104:094102.
[55] Huang X, Jiao F, Zhang C, Chen Y, Xie Y, Xie W. Investigation of polymeric CO synthesized at high pressure and its stability under ambient conditions: a first-principles study. J Phys Chem C 2022;126:19571–9.
[56] Kondrin M, Lebed Y, Brazhkin V. A new polymorph of graphene monoxide: an all-sp 3 bonded metal and ambient pressure superconductor. CrystEngComm 2023;25:1328–32.
[57] Scuseria GE, Miller MD, Jensen F, Geertsen J. The dipole moment of carbon monoxide. J Chem Phys 1991;94:6660–3.